Discover Materials

Discover

Review

The differences in crystal structure and phase of lead-free perovskite solar cell materials

Samuel R. Pering[1]

Received: 7 June 2023 / Accepted: 6 July 2023
Published online: 22 August 2023

Abstract
Hybrid organic–inorganic lead halide perovskite materials have established themselves as a competitive solar cell technology, with high efficiencies and simple processing. However the main drawback of these materials is currently their stability, which is complicated by the potential to release the toxic element lead into the environment. Attempts to replace lead for less-toxic starting materials have generated significant research interest. Any candidate material must have enhanced stability and comparable performance to lead halide perovskites, and an understanding of the structure is key to developing these materials to be competitive. This review provides a brief overview and reference of experimentally determined crystal structures of lead-free perovskite materials. The most promising potential materials are identified as those that maintain a cubic structure, particularly double-perovskite type absorbers.

1 Perovskite solar cell introduction

The discovery of hybrid organic–inorganic lead-halide materials' photovoltaic activity has led to a significant new area of research: Perovskite Solar Cells (PSC) [1]. This term is used for solar cell absorber materials that possess the perovskite crystal structure, originally based on $CaTiO_3$ [2]. During their research journey, perovskite materials have found themselves to have many commercially beneficial properties, *e.g.*: abundant starting materials, simple processing methods, [3–5] and low energy costs of device production [6, 7]. Recently progress has been made in upscaling PSC device production, the solution processable nature of the starting materials lending itself to printing the absorber layer [8–10].

Perovskite solar cell efficiencies have also increased greatly since their inception in 2009, efficiencies of over 25% have now been recorded, making them competitive with commercially available technologies [1, 11]. One of the key developments that has increased cell efficiency is changing the ABX_3 components from the original methylammonium (MA) lead iodide [1]. Through the use of additives such as formamidinium (FA), [12–14] caesium [15–18], among many others in various combinations [19–24], the structure and band gap can be altered to produce desirable efficiency and stability improvements [25–27]. A more pronounced band gap change is observed when the halide anion is mixed; varying the ratio of iodide to bromide can lead to colour control from black, to red and yellow [28, 29].

One constant feature of high-performance perovskite solar cells has been the cation that occupies the B-site of the perovskite, lead. Whilst minimal amounts of lead are used—and indeed it is not the largest environmental cost of manufacture, which is currently the device fabrication procedures—studies have shown that lead leached into the environment from perovskite solar cells can be taken up by organisms in nature [6, 30–34]. This is exacerbated by the current long-term stability of perovskite absorber materials. Degradation mechanisms of the absorber material can be triggered by

✉ Samuel R. Pering, s.r.pering@lboro.ac.uk | [1]Department of Materials, Loughborough University, Loughborough LE11 3TU, UK.

heat, [35, 36] moisture [37], and light [38, 39]. Not only is this detrimental to device performance, but also increases the chances of lead being released into the environment through water soluble lead being washed away from the cells [40].

Tactics to improve the stability are currently manifold. The first of these is to alter the structure of the perovskite itself to prevent degradation through substitution. Previous studies have shown that cations of various size can be incorporated into the perovskite structure; Low molar ratio substitutions at the A, B and X sites can lead to significant improvements in performance and stability [23, 41]. However by altering the ions used, the crystal structure of the perovskite material can undergo significant changes, which can be predicted using the Goldschmidt tolerance factor. The tolerance factor predicts the viability of a combination of A, B and X components for the formation of a perovskite phase by calculating a structural ratio; a value between 0.9 and 1.0 would predict a cubic perovskite to form and can be calculated in different ways, for example including octahedral factor corrections to address changes in metal-halide bonding [42–45]. As an example using the most basic approach, methylammonium lead iodide (Tolerance factor 0.9) possesses a tetragonal (I4/mcm) perovskite structure at room temperature, transitioning to cubic/pseudocubic at higher temperature and hexagonal at low temperatures, as shown in Fig. 1 [46]. Formamidinium lead iodide (Tolerance factor 1.03) has a cubic ($Pm\bar{3}m$) structure in its black phase [47]. Weber et al. showed that a mixture of formamidinium and methylammonium as the A-site cation can form a continuous solid solution at various ratios of formamidinium:methylammonium, demonstrating phase change from tetragonal to cubic [48].

The ability to control the structure through ion substitutions is particularly important in the case of formamidinium lead iodide, which readily degrades into a non-photoactive δ-phase at room temperature [14, 47]. Stabilising the photoactive cubic phase through substitutions of bromide, caesium and methylammonium is what forms the state-of-the-art triple cation perovskite, $Cs_{0.05}(FA_{0.83}MA_{0.17})_{0.95}Pb(I_{0.83}Br_{0.17})_3$, hence understanding the structure of perovskite materials is vital in developing high-performance devices [41]. The importance of the higher symmetry cubic phase in $FAPbI_3$ is obvious, with the associated change in colour and therefore band gap, and photoactivity. The formation of cubic structures as opposed to lower symmetry tetragonal or hexagonal structures in perovskite materials leads to many differences [51]. While it has been found that the tetragonal-cubic phase change through temperature does not contribute to a significant change in band gap [52], controlling the metal-halide bond distance chemically does; controlling the band gap to be closest to the ideal thermodynamic efficiency limit value of 1.34 eV will enable improved performances [28, 53]. The increased disorder of the methylammonium cation in the cubic phase could impact charge transport [54], has been attributed to performance increases, although it may affect overall stability [50, 55–58].

For enhancing perovskite stability, if the A-site cation substituted in is large enough, it can cause the separation of the structure into distinct 2D, 1D or 0D perovskites [59–62]. 2-Dimensional perovskites consist of layers of lead-halide octahedra separated by the large organic cation, which can act as a buffer layer preventing degradation—such techniques have been used to create devices that are stable over a year [63, 64].

A second method for improving cell stability, and therefore preventing lead egress, is to alter the device architecture. Using a porous carbon electrode that can be backfilled with the absorber not only improves humidity resistance, it also means significantly less starting material is required (compared to *e.g.* spin-coating) [65–67]. Carbon-electrode perovskite solar cells have been demonstrated to maintain stability over 1000 h [68].

Lead sequestration, using a chemical approach to absorb any lead lost from the perovskite material is a growing area of research that aims to prevent lead being lost to the environment [69]. This can be achieved through the including phosphate salts within the perovskite material itself, that form a water insoluble salt with lead that prevents it washing into the environment [70]. Alternatively interlayers or encapsulants that absorb lead can be used; which have shown no

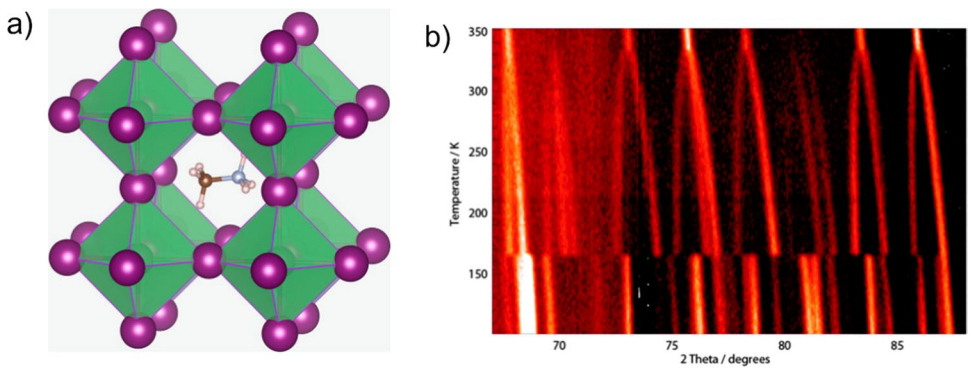

Fig. 1 **a** The tetragonal crystal structure of methylammonium lead halide, reproduced with permission from reference [49] and **b** PXRD demonstrating the phase changes with temperature, reproduced from reference [50] with the permission of the Royal Society of Chemistry

impact on optoelectronic properties, and been able to significantly reduce any lead contamination [71, 72]. It has also been found that soil can effectively sequester lead—however some remains available to biological organisms within it. [73]

Perhaps the simplest way to prevent lead being lost into the environment is to use alternative materials; the challenge within is to maintain the beneficial structure and properties of the lead-based perovskite materials. Figure 2a shows a pictorial representation of the alternative elements explored so far. In this review the structure of different lead-free perovskite materials will be summarised, with a focus on those synthesised and determined experimentally. Lead-free perovskites are a growing research topic within the perovskite solar cell community, and have seen a rise in publications since 2016 (Fig. 2b). At the start of each section a table is provided containing the abundance of the material and information on its toxicity, taken from materials safety data sheet information. Where data is not available, this does not necessarily mean they are non-toxic, it is that there is no data on these materials yet.

2 Group 14

As it is in the same group as lead, and only one row up in the periodic table, tin was the obvious first choice to replace lead in perovskite solar cell materials, and is currently the most extensively studied replacement. Tin possesses a similar ionic radius to lead, hence using tolerance factor as a guide can form a perovskite with many of the components already used in lead-based perovskite materials [44, 75, 76]. Although tin is an abundant element, it is less so than lead, resulting in more expensive starting materials which would lower the effect of a key advantage of perovskite solar cells, their relatively low cost of production. There are also concerns about the environmental safety

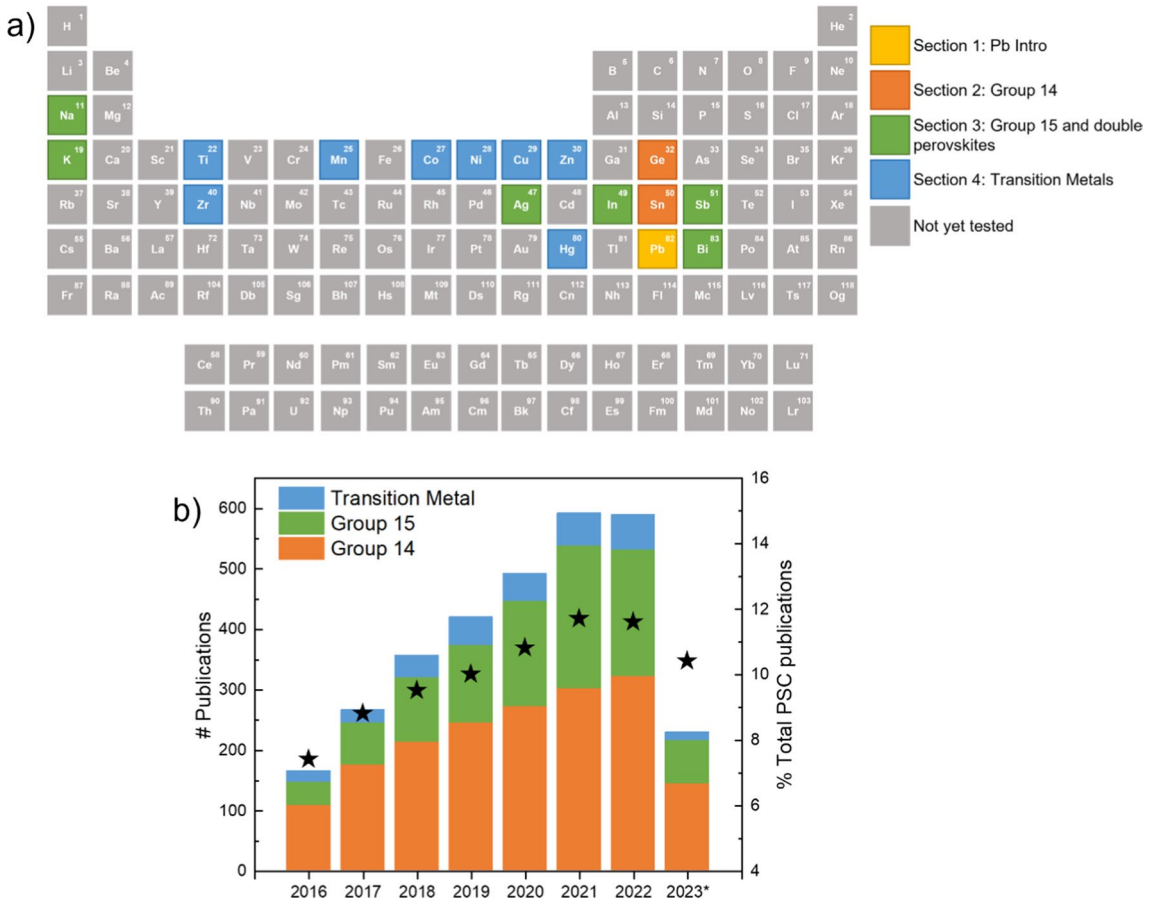

Fig. 2 **a** Periodic Table of the Elements. B-site elements discussed in this review are highlighted with respect to their relevant section and **b** representation of lead-free publications related to each group with starred value representing percentage of 'lead-free' perovskite solar cell publications compared to total perovskite solar cell literature, data taken from Web of Science—data for 2023 until June 2023

Table 1 Abundance and toxicity of elements discussed in "Group 14" Section, with lead included

Element	Abundance (ppm in Earth's crust)[74]	Toxicity	
		Occupational exposure limit to metal iodide salt (mg/m^3)	LD50 (Oral) (mg/kg)
Lead	14	0.15	500
Tin	2.3	4	2274
Germanium	1.5	No data available	No data available

Data for toxicity taken from SDS data (Merck) for metal iodide salts and HSE.gov.uk where available

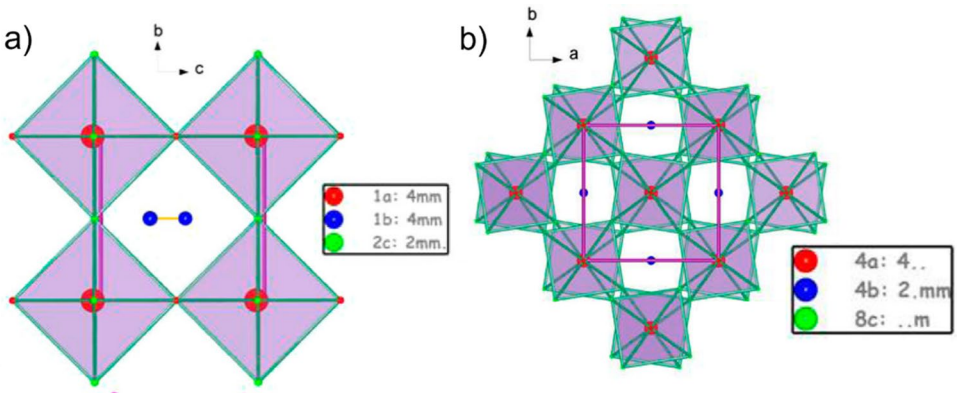

Fig. 3 Unit cells of the **a** α-phase and **b** β-phase of $MASnI_3$ and $MAPbI_3$. Reprinted (adapted) with permission from C. C. Stoumpos, C. D. Malliakas, and M. G. Kanatzidis, Inorg. Chem., 2013, 52, 9019–9038. Copyright 2013 American Chemical Society

of tin-perovskite materials, showing similar toxicity to lead-based materials (Table 1), although the bioavailability of tin upon leakage into the environment has been demonstrated to be much lower than lead [31, 77]. Taking an additional step up group 14 in the periodic table brings you to another potential substitute for lead in germanium, an element even less abundant, with a significantly smaller ionic radius [44, 75]. Germanium does have fewer environmental concerns than both tin and lead [78].

Before their application in photovoltaics, organic tin-halide perovskites had been identified as potentially interesting materials for similar reasons to those for lead; that they are low cost, require simple processing methods and possess good transport properties [79, 80]. Early tin-halide perovskites tended to be lower dimensionality, with larger cations included to improve stability [79, 81]. The reduced charge transport capabilities inherent in lower dimensionality perovskite materials perhaps impeded the application of tin-halide perovskites for photovoltaics.

$CsSnI_3$ is one of the earliest recorded tin perovskites used in a solar cell—in this case a Schottky cell with no transport materials that exhibited 0.9% efficiency [82]. At room temperature $CsSnI_3$ possesses an orthorhombic structure; a cubic structure is formed by X-site substitution to bromide (a monoclinic structure is made by $CsSnCl_3$) [83–85]. High temperatures of over 150 °C are required to transition $CsSnI_3$ into a cubic phase [83]. By switching from caesium to methylammonium, and incorporating the tin-perovskite absorber layer into a mesoporous titania scaffold, efficiencies of over 6% could be attained [86]. The structure of methylammonium tin halide perovskites shows similar trends to some of their lead-analogues, *i.e.* there is a hexagonal phase and a cubic black perovskite phase; these transitions are displayed in Fig. 3 [87].

Both $MASnI_3$ and $MAPbI_3$ possess orthorhombic, tetragonal and cubic phases—$MASnI_3$ exists in the tetragonal (P4mm) structure at room temperature, with remarkably similar lattice parameters to $MAPbI_3$ [50, 86–88]. The tetragonal-cubic phase transition occurs at a slightly lower temperature for $MASnI_3$, at around 20 °C [89]. Possessing phase-transition temperatures within the expected range a photovoltaic device may be expected to endure is not ideal, as it can affect properties such as resistivity [89]. Interestingly, methylammonium tin iodide has been found to have some metallic properties, as opposed to being purely semiconducting [80, 90]. This has been attributed to hole-doping that occurs during material crystallisation and degradation to metallic tin [89, 91]. As is the case when Cs^+ is the A-site cation, using bromide instead of iodide produces a material with a cubic structure [92]. Single crystals of formamidinium tin iodide have also been synthesised, which are orthorhombic at room temperature (space group Amm2), and as expected for a larger cation show a slightly expansion of the lattice compared to methylammonium [87, 93].

Currently, a significant barrier to more widespread research of tin-based materials is the rapid degradation caused by the tin cation greatly preferring the + 4 oxidation state [87, 94, 95]. Issues of material stability have been addressed in lead-based materials by the formation of 2D materials or through surface passivation [96–99]. Such phases can be formed with tin in the B-site using bulky organic cations such as phenylethenammonium (PEA); issues of charge transport inherent in materials where the inorganic backbone is disrupted were reduced slightly through artificial hole doping [100, 101]. Degradation to the + 4 oxidation state can also be slowed through other means. Using $NABH_4$, a reducing agent, as an additive tin-perovskite materials based on $FASnI_3$ have been engineered to be stable for over 1000 h, with an initial efficiency of ~ 9% [102].

The next row up in the periodic table from tin is germanium – although germanium possesses a significantly smaller ionic radius than lead, at 73 pm compared to 119 pm. The result of this is that germanium iodide perovskites $CsGeI_3$, $MAGeI_3$ and $FAGeI_3$ exhibit a trigonal/rhombohedral (space group R3m) structure, shown in Fig. 4 [103–106]. $CsGeI_3$ undergoes a phase transition to a cubic structure at 277 °C; if the iodide is substituted to chloride ions the phase transition temperature is brought below 200 °C [105]. Reducing the size of the X-site anion also reduces the phase transition temperature in lead-based perovskites [107]. A further similarity can be found when using large A-site cations, similar manipulation of the dimensionality of the structure can be obtained. 2D-perovskites can be formed when an A-site cation such as *n*-butylammonium is used, overall producing an orthorhombic structure of germanium iodide sheets separated by the organic cation [100]. Stoumpos et al.'s analysis of the structure of germanium based perovskites also discovered the presence of 1D perovskite structures when using organic cations such as guanidinium (Fig. 4c) and trimethylammonium [104]. Germanium based materials are sparsely investigated, likely due to the increased instability of the + 2 state (even compared to tin).

An alternative approach to the problem of metal cation oxidation is to produce materials that rely on the B-site cation being in its more stable + 4 oxidation state to begin with. Materials such as Cs_2SnI_6 (which is the degradation product of $CsSnI_3$) [87] form vacancy ordered double perovskites, illustrated in Fig. 5, a structure which essentially involves the removal of every other B-site cation [108, 109]. This is based on the antifluorite structure exhibited by *e.g.* Na_2O—however

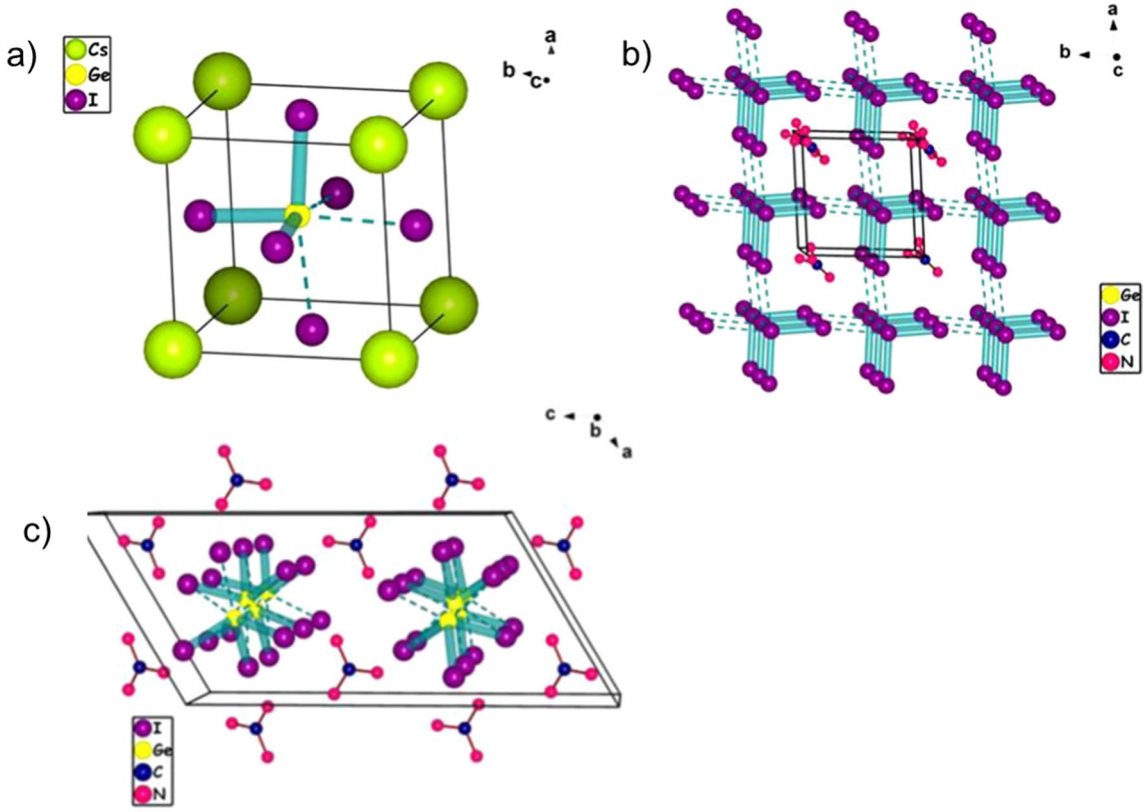

Fig. 4 Trigonal Germanium structures, **a** $CsGeI_3$, **b** $FAGeI_3$ and **a** $GAGeI_3$. Reprinted (adapted) with permission from C. C. Stoumpos, L. Frazer, D. J. Clark, Y. S. Kim, S. H. Rhim, A. J. Freeman, J. B. Ketterson, J. I. Jang, and M. G. Kanatzidis, J. Am. Chem. Soc., 2015, **137**, 6804–6819. Copyright 2015 American Chemical Society

double perovskite has become a common term for this particular structure in photovoltaic literature. Usefully tolerance factor calculations can still be applicable when looking at double-perovskites [110]. Standard double-perovskites possess a cubic structure of space group Fm $\bar{3}$ m [111].

While A_2BX_6 materials have been less well investigated than ABX_3 (or indeed $A_2B'B''X_6$), some structural analysis and variation of the crystal structure has been performed. Most tend to exhibit the same cubic structure as Cs_2SnI_6, this structure is preserved with halide substitution in the Cs-containing material [112, 113]. Hybrid organic–inorganic double perovskites have also been synthesised, MA_2SnI_6, MA_2SnBr_6 and MA_2SnCl_6 all form the standard cubic structure for this class of materials, with a slightly expanded lattice compared to caesium [112, 114]. The only experimentally determined exception to the cubic structure, Rb_2SnI_6 forms a tetragonal structure (P4/mnc) at room temperature which transitions to a monoclinic lattice at low temperatures (< 120 K) [115, 116]. At the time of writing no equivalent materials using germanium have been synthesised, although computational calculations suggest that germanium iodide double perovskites would have suitable band gaps for single-junction solar cells [117].

2.1 Summary

The focus of using group 14 elements has been as a straight replacement for Pb, although currently Sn and Ge based materials have shown similar problems with stability and toxicity, with no efficiency improvements to compensate. Vacancy-ordered double perovskite materials may be an advantageous use of tin: these materials tend to exhibit high stability, and many have appropriate band gaps [108, 118]. While they have currently been employed as hole conductors rather than absorber layers, options for band-gap engineering could widen the possible application of these materials [119, 120].

3 Group 15 and double perovskites

Taking one step to the right of the periodic table from lead comes to bismuth, which has been studied as a potential substitute to lead as it has a similar electronic configuration and has been assessed to be less environmentally damaging (Table 2) [121]. For Group 15 materials, the + 3 oxidation state is the most favoured for elements such as bismuth and antimony, so the perovskite structure must accommodate this. This means a different ratio of A:B:X ions is prevalent. Importantly, the ionic radii of bismuth alongside other typical ions used in perovskites for photovoltaics fit tolerance factor calculations of what may produce a viable perovskite [122].

Perovskite materials based on Bismuth Iodide as the B and X ions generally possess a deep red colour; revealing a larger band gap in the above 1.9 eV. Single crystals made of methylammonium bismuth iodide and caesium bismuth iodide show the same structure. Hexagonal crystals are formed of space group $P6_3/mmc$, in which two face-sharing octahedra of bismuth iodide, $[Bi_2I_9]$ [3–] are neutralised by three surrounding methylammonium or caesium cations, shown in Fig. 6 [123–126]. The short bismuth to bismuth distance involved leads to some structural distortion in the face-sharing octahedra of methylammonium bismuth iodide [123]. This type of structure is referred to as zero-dimensional, as there is no continuation in any axis direction. Changes to the crystal structure are observed when reducing the size of the A-site

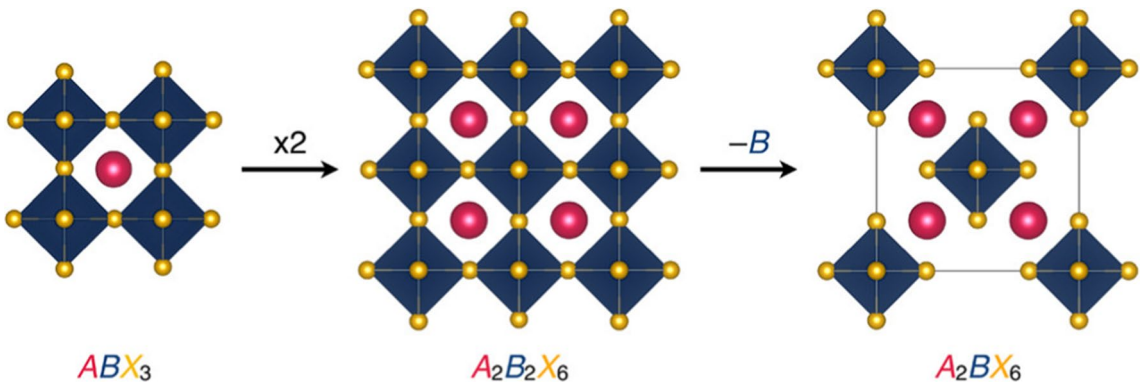

Fig. 5 A visual demonstration of the vacancy ordered double perovskite structure. Reprinted (adapted) with permission from A. E. Maughan, A. M. Ganose, D. O. Scanlon, and J. R. Neilson, Chem. Mater., 2019, **31**, 1184–1195. Copyright 2019 American Chemical Society

Table 2 Abundance and toxicity of elements discussed in "Group 15 and double perovskites" Section, with lead included.

Element	Abundance (ppm in Earth's crust)[74]	Toxicity	
		Occupational exposure limit (metal iodide salt) (mg/m^3)	LD50 (Oral) (mg/kg)
Lead	14	0.15	500
Bismuth	0.0085	No data available	No data available
Antimony	0.2	0.5	No data available
Silver	0.075	No data available	No data available
Indium	0.25	0.1	No data available
Sodium	23,600	No data available	4340
Potassium	20,900	No data available	No data available

Data for Exposure limits taken from SDS data (Merck) for the most relevant metal iodide salt and HSE.gov.uk where available. Elements with lower limits than lead highlighted in red

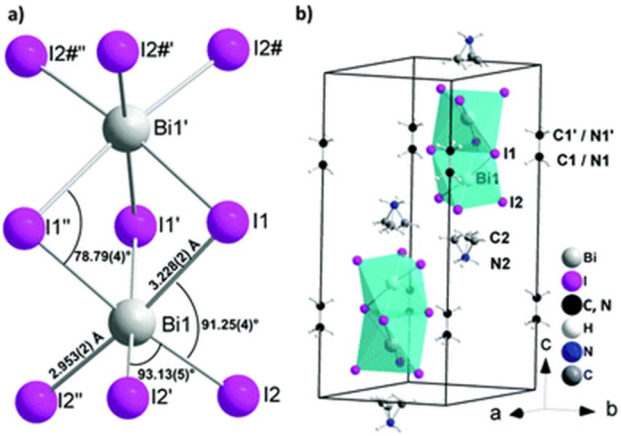

Fig. 6 The structure of Methylammonium Bismuth Iodide, $MA_3Bi_2I_9$. Reproduced from Ref. 99 with permission from the Royal Society of Chemistry

cation to ammonium/rubidium, or when reducing the size of the X-site anion to bromine. The structure of ammonium bismuth iodide was analysed by Sun et al. to be monoclinic; it also had a marginally lower band gap than methylammonium bismuth bromide at 2.04 eV [127]. Rubidium bismuth iodide also produced a monoclinic crystal structure [128]. When replacing the iodide anion in methylammonium bismuth iodide with bromide, the single crystal structure changes; there are no longer face-sharing octahedra, individual $[BiBr_6]^{3-}$ units are formed, with three methylammonium ions [127]. Solar cells made using only bismuth as the B-site ion have shown some photovoltaic activity, but efficiencies still remain below 1% [122, 129–131]. The stability of these materials is however improved compared to lead [132].

Antimony has also been investigated as the B-site anion, and has shown marginally higher efficiencies when used in solar cells compared to analogous bismuth materials [133–135]. Antimony-based perovskite materials share a 0D structure with bismuth, furthermore $MA_3Sb_2I_9$ and $(NH_3)_3Sb_2I_9$ show same hexagonal and monoclinic structures respectively to their bismuth analogues [133, 134]. $Rb_3Sb_2I_9$ is also monoclinic, and was found to create more ordered layers of octahedra in the bulk material compared to an equivalent material using cesium [135]. It should however be noted that antimony is also highly toxic, so does not immediately solve the problems presented by using lead-based materials [136, 137].

Formation of a double perovskite structure can be achieved through the addition of a second, B′ cation to the mixture [138]. Previously we have looked at vacancy-ordered double perovskites when using B-site cations which strongly favour the + 4 oxidation state. The following double-perovskite materials all use a combination of two different cations, one in its + 3 oxidation state and another in a + 1 oxidation state, with a general formula $A_2B'B''X_6$ [138–140]. Iodobismuthate structures are potentially the most exciting of the lead replacement opportunities, as $AgBi_2I_7$, which forms a cubic structure, produces cells which have reached efficiencies of > 4% in thin-film solar cells [141, 142]. Silver bismuth materials have also found success when synthesised as quantum dots, which has the potential to create new ways to deploy solar cell technologies [143–146]. While the synthesis, composition and shape of individual quantum dots can vary significantly, [139] this review is focussed on the structure of the bulk materials.

As mentioned with the tin-based perovskites, double-perovskites based on an $A_2B'B''X_6$ exhibit a cubic structure. While there is a large amount of possible substitution in $A_2B'B''X_6$, those with silver and bismuth in the B' and B'' position respectively share an Fm $\bar{3}$ m space group [147–149]. $Cs_2AgBiBr_6$ is the most extensively studied of these materials—see Fig. 5 for general structure (analogous Fm3m structure to $A_2B_2X_6$) [150]—and currently produces cells with ~ 2.5% efficiency [149, 151]. The metal halide backbone of $Cs_2AgBiBr_6$ ideally consists of alternating octahedra with bismuth and silver at the centre; however defects and vacancies produced during synthesis can lead to disorder in $A_2B'B''X_6$ type materials, producing changes in properties such as the band gap [149, 152–154]. Another common feature of silver-bismuth double perovskites to their lead and tin counterparts is the presence of a phase-transition from tetragonal to cubic. In the case of $Cs_2AgBiBr_6$, this transition happens well below room temperature, at ~ 120 K [155]. The temperature of this phase transition can be altered by a few degrees Kelvin through partial substitution at the A-site with alkali metal cations such as rubidium and sodium [148]. Such substitutions were also found to have minimal effect on the overall lattice parameters.

In the context of perovskite solar cells, which typically use low cost starting materials, silver is relatively expensive, and so alternatives for the B' site have been investigated. As alkali metals form ions with a suitable + 1 charge, they can also inhabit the B' position on a double perovskite. Additionally halide salts of these elements are generally abundant and cheap. $Cs_2NaBiCl_6$ possesses the same cubic structure as $Cs_2AgBiBr_6$ [147]. One step down the group with potassium, $(MA)_2KBiCl_6$ forms a rhombohedral structure R $\bar{3}$ m, with corner sharing KCl_6 and $BiCl_6$ octahedra in a 3D network [156]. Copper, as the element above silver in the periodic table, is another viable candidate. However the starting materials CuCl, CuBr, and CuI all are hazardous to the environment. If the main goal of discovering new perovskite solar cell compounds is to alleviate the toxicity problems inherent with lead, alternative starting materials should also be critically analysed. Although copper has been predicted computationally to form a double perovskite with bismuth, at the time of writing no A_2CuBiX_6 compounds have been synthesised [138, 157, 158].

Double perovskites can also be produced with indium as a substitute to bismuth, in $Cs_2AgInCl_6$ the same cubic structure is formed, however the band gap at over 3.3 eV would not be suitable for photovoltaic applications [159]. $Cs_2NaGaBr_6$ and $Cs_2LiGaBr_6$ have been computationally identified as potentially suitable materials with band gaps of 1.76 and 1.97 eV respectively [160].

3.1 Summary

Group 15 perovskite materials mainly feature bismuth. As a replacement to the readily available lead, there are issues of abundance and starting material cost that need to be considered when employing bismuth, or indeed antimony, based materials. There is a significant variety in potential materials; standard, single B-site perovskites tend to exist in lower dimensionalities which will likely cause issues with charge transport within the absorber layer. Double perovskites are a good alternative that possess an ordered, cubic structure and a continuous inorganic backbone. These materials typically have higher band gaps, so additional band-gap engineering should be explored, or they could be used in other devices such as LEDs or photodetectors [152, 161].

4 Transition metals

Transition metals would be an ideal substitute for lead-based compounds, as top-row transition metals are largely abundant (Table 3). Titanium, iron, manganese, zinc, cobalt, nickel, zirconium, calcium and magnesium can possess suitable oxidation states, and a number of computational studies have identified a series of transition and group 2 metal perovskites as having significant potential for high-efficiency devices [162–167]. Computational calculations have facilitated more targeted experimental synthesis of single and double perovskites, and can also provide information to aid transport layer selection (by calculating conduction band and valence band energies) [163]. For example in the work by Jacobs et al., after generating potential perovskite materials their measurements firstly refine for thermodynamic stability, before refining based on band-gap, and finally solar cell efficiency. From computational calculations, materials using the relatively abundant magnesium and iron as the B-site ion have been found to have suitable structures (crystal structures of various magnesium perovskites using different A-site cations are shown in Fig. 7). $KFeI_3$ was identified as a material that could reach efficiencies of over 24% [162]. However when simple, solution based synthesis was attempted, no material was formed; such materials may require more intense synthesis methods [168]. For example $Cs_3Fe_2Br_9$ was synthesised in an autoclave for 3 days [169]. This formed a hexagonal, zero-dimensional perovskite ($P6_3/mmc$) similar to bismuth analogues, except with a more suitable band gap for

Table 3 Abundance and toxicity of elements discussed in "Transition metals" Section, with lead included.

Element	Abundance (ppm in Earth's crust)[74]	Toxicity	
		Occupational exposure limit (metal iodide salt) (mg/m^3)	LD50 (Oral) (mg/kg)
Lead	14	0.15	500
Zinc	70	No data available	No data available
Copper	60	1	2000
Mercury	0.085	0.02	18
Nickel	84	No data available	No data available
Cobalt	25	0.1	406
Manganese	950	0.05	No data available
Titanium	5650	No data available	No data available
Zirconium	165	5	No data available

Data for toxicity taken from SDS data (Merck) for the most relevant metal iodide salt (data for cobalt is taken from cobalt bromide) and HSE.gov.uk where available. Elements with lower limits than lead highlighted in red

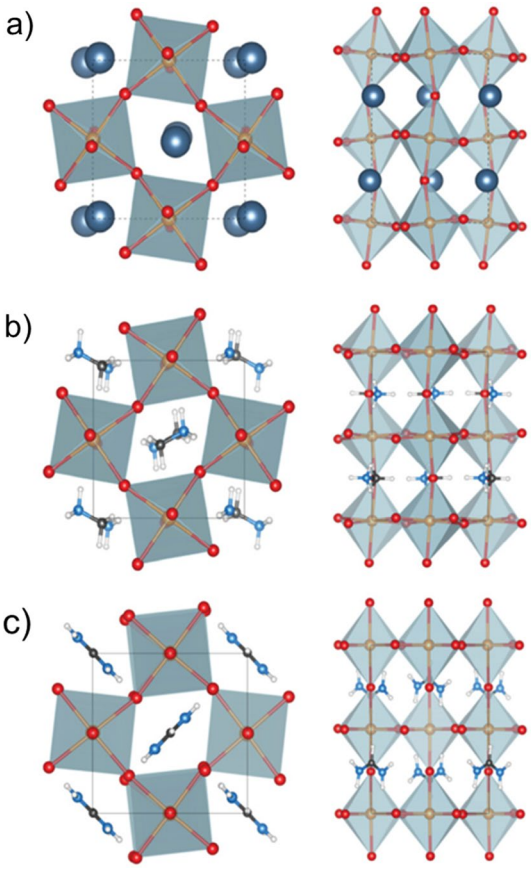

Fig. 7 Crystal structures of the computationally generated magnesium halides **a** $CsMgI_3$, **b** $MAMgI_3$ and **c** $FAMgI_3$ materials. Reprinted (adapted) with permission from M. R. Filip and F. Giustino, J. Phys. Chem. C, 2016, **120**, 166–173. Copyright 2016 American Chemical Society

photovoltaics of 1.65 eV. Due to the abundant nature of iron, such materials would be a useful avenue of further research.

While transition metal perovskites have not yet been widely explored compared to group 14 and double-perovskite based alternatives to lead, there have been some promising initial experimental findings with manganese, titanium and copper as lead-replacements [170–178].

In the 'original' perovskite, $CaTiO_3$, titanium is in its + 4 oxidation state. This is also true of titanium halide perovskites for solar cells, which mostly follow the same cubic vacancy-ordered double perovskite structure, A_2TiX_6, shown in Fig. 5

[179]. Perovskite materials with titanium in the + 2 oxidation state have been synthesised, $RbTiBr_3$ and $CsTiBr_3$ both forming a hexagonal perovskite, although there have been few follow-up studies on optoelectronic properties or photovoltaic performance [179, 180]. Computational studies have suggested that both double perovskite Cs_2TiX_6 and $ATiX_3$ materials may show good PV activity when paired with the correct transport layers [181, 182].

Fully inorganic Cs_2TiBr_6 is the most well studied of the vacancy-ordered double perovskite titanium materials, with a band gap of 1.82 eV and an experimental efficiency of 3.3% [172, 183]. Although compared to an equivalent band-gap lead-based perovskite it has been shown that Cs_2TiBr_6 is relatively stable to heat and light, [172] unfortunately it still degrades rapidly in air leading to the formation of the CsBr starting material peak on a timescale of 1–2 h [184, 185].

While mostly studied as a dopant (including in bismuth perovskites), [186–188] perovskites using manganese as the sole B-site cation have also been synthesised [189]. Methylammonium manganese bromide ($MAMnBr_3$) possesses a hexagonal perovskite structure, which on exposure to moisture forms a hydrated monoclinic structure in the same manner as hydrated $MAMnCl_3$ and hydrated $CsMnCl_3$, shown in Fig. 8 [170, 190]. Using chloride anions can also produce a metal-poor MA_2MnCl_4 material that exists in an orthorhombic structure [170, 191]. Switching to the much larger iodide cation produces an orthorhombic compound with a tetrahedral coordination of the Mn^{2+} ion (Space group Pbca, Fig. 8b), [170] however manganese iodide as a starting material is still environmentally toxic.

In the same work, Daub et al. investigated various nickel-based perovskite materials [170]. Caesium and potassium nickel halides had been previously analysed to exhibit hexagonal perovskite structures [192, 193]. When increasing the size of the A-site cation to methylammonium, an orthorhombic structure is formed [194, 195]. Exposure of these materials to moisture leads to the formation of 1-dimensional hydrated structures, which consist of chains of corner sharing octahedra that rely on hydrogen bonding to co-ordinate the separate chains. The water molecules involved cause an ~ 125° to form between octahedra [170]. Such hydrated structures possess a monoclinic perovskite structure [190].

A detailed structural study of methylammonium cobalt halide materials found that $(CH_3NH_3)_2CoX_4$ also generally crystallised as a monoclinic structure [196]. However in this case cobalt halide octahedra are not formed—instead the material has $[CoX_4]^{2-}$ *tetrahedra*.

Similar structures have been discovered when using mercury or zinc as the metal [197, 198]. These tetrahedra do not share a corner or a face, and are stacked in the same orientation in the c axis. This structure holds when mixing chloride and bromide anions, and with mixed bromide/iodide materials. 100% iodide containing compounds, and iodide mixed with chloride show two different structures, orthorhombic and an undefinable structure based on distorted hexagonal layers respectively.

Copper can also exist in appropriate oxidation states for perovskite formation and can show significant variance in crystal structure depending on the A or X-site cations used, or synthesis method of the crystal [199–201]. Partial

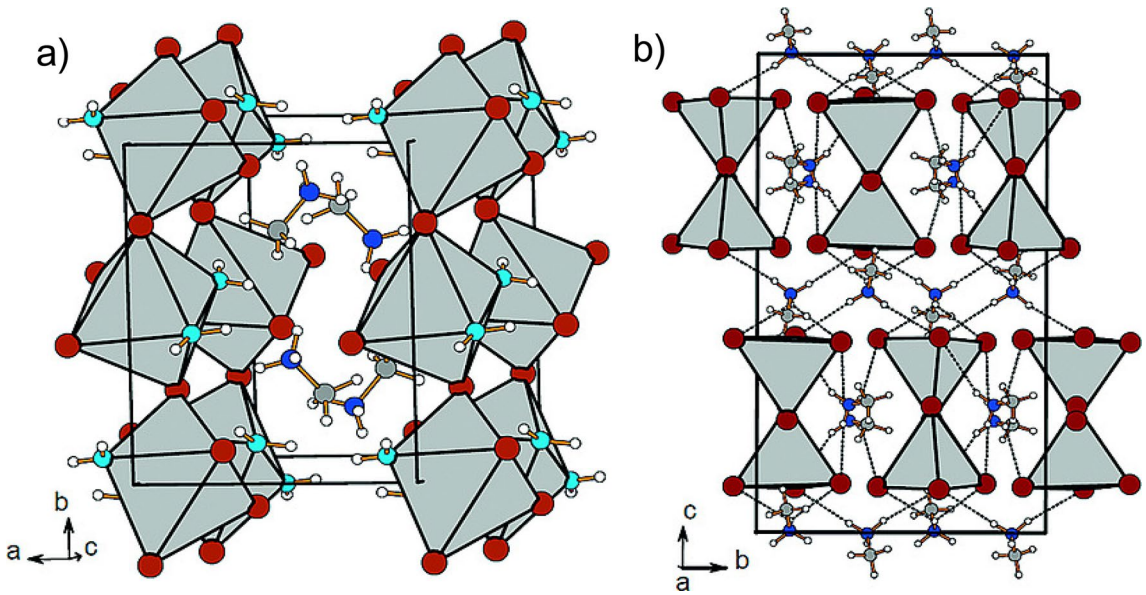

Fig. 8 **a**The hydrated structure of $MAMnBr_3(H_2O)_2$ and **b** the crystal structure of MA_2MnI_4. Reproduced and Adapted from Reference 145, M. Daub, I. Ketterer, and H. Hillebrecht, *Zeitschrift für Anorg. und Allg. Chemie,* 2018, **644**, 280–287 © 2018 WILEY–VCH Verlag GmbH & Co. KGaA, Weinheim

Table 4 A summary of some materials of interest looked at throughout the report, grouped by crystal structure and highlighted in the colour of the corresponding section

Structure	Material	Space group	Band gap (eV)	Efficiency (%)
Cubic	Cs_2SnI_6	$Fm3m$[112]	1.26[112]	4.23[112]
	$Cs_2AgBiBr_6$	$Fm3m$[206]	2.0[207]	3.11[208]
	Cs_2TiBr_6	$Fm3m$[183]	1.8[172]	3.2[172]
Hexagonal	$MA_3Bi_2I_9$	$P6_3/mmc$[123]	1.96[123]	
	$MA_3Sb_2I_9$	$P6_3/mmc$[133]	2.14[133]	0.43[133]
	$Cs_3Fe_2Br_9$	$P6_3/mmc$[169]	1.65[169]	-
Tetragonal	$MASnI_3$	$P4mm$[87]	1.23[86]	6.4[86]
Trigonal	$MAGeI_3$	$R3m$[104]	1.9[104]	0.3%[205]
Orthorhombic	$FASnI_3$	$Amm2$[87]	1.41[87]	9%[102]
Monoclinic	MA_2CuCl_4	$P2_1/a$[202]	2.36[177]	2.41[177]

substitution of bromide into methylammonium copper chloride materials causes a lattice change from monoclinic to orthorhombic, accompanied by a significant change in the *c* lattice parameter compared to pure chloride, from 9.97 to 19.1 Å for a material containing 50% bromide [201]. It is the pure chloride methylammonium copper perovskite (exhibiting a monoclinic $P2_1/a$ structure) [202] that has so far shown the greatest photovoltaic efficiency at 2.41%; in this case (unlike with lead analogues) substitution of bromide or iodide serves to reduce the efficiency [177]. Caesium copper halides tend to form in the orthorhombic Pnma structure, unless synthesised at room temperature at which point a tetragonal (I4/mmm) structure is formed [200]. The only second row transition metal that has been analysed at the time of writing, is Zirconium—which also forms a double perovskite structure [203, 204]. While nanocrystals of Cs_2ZrCl_6 and Cs_2ZrBr_6 were found to be phase pure, bulk powders contained a degree of impurity phases [203].

4.1 Summary

While some transition metal replacements for lead would be beneficial due to relative abundance, cost and low-toxicity, they don't regularly form the structures that have been shown to be most beneficial for photovoltaic performance. Further to this transition metal perovskites tend to exhibit wide-bandgaps, which would not be suitable for high-efficiency single junction devices, but may find some use in multijunction solar cells.

5 Future outlook/conclusions

The most efficient lead-based perovskite materials generally possess a cubic structure. Table 4 shows a summary of some materials of interest throughout the report grouped by crystal structure. Of the materials discussed in this review, some tin materials and the 'double perovskite' materials all show the same cubic structure, and may be more relevant for future research than the strained/distorted trigonal or hexagonal structures shown by germanium and manganese respectively. Particularly those materials such as Cs_2SnI_6 in which the B-site cation is already in its more stable, +4 oxidation state may be of significant interest. Also band-gap engineering through the inclusion of multiple A-site or X-site cations on tin-based materials should be examined. On the topic of stability, lower-dimensional perovskites when using a suitable A-site cation can cause a longer lifetime in perovskite materials, however long-term studies of such lead-free materials are yet to be performed. Finally, there are a large number of potential perovskite materials that have been identified by computational studies but not yet synthesised. Attempting to produce these materials would generate broader knowledge of the material class as a whole, and help determine the viability of lead-free perovskite materials.

Acknowledgements S.R. Pering thanks Loughborough University for funding.

Author contributions S.P. wrote and edited manuscript.

Declarations

Competing interests The authors declare no competing interests.

References

1. Kojima A, Teshima K, Shirai Y, Miyasaka T. Organometal halide perovskites as visible-light sensitizers for photovoltaic cells. J Am Chem Soc. 2009;131:6050–1.
2. Kay HF, Bailey PC. Structure and properties of CaTiO3. Acta Crystallogr. 1957;10:219–26.
3. Ball JM, Lee MM, Hey A, Snaith HJ. Low-temperature processed meso-superstructured to thin-film perovskite solar cells. Energy Environ Sci. 2013;6:1739–43.
4. Heo JH, Im SH. Highly reproducible, efficient hysteresis-less CH3NH3PbI3-xClx planar hybrid solar cells without requiring heat-treatment. Nanoscale. 2016. https://doi.org/10.1039/C5NR08458J.
5. Casaluci S, et al. A simple approach for the fabrication of perovskite solar cells in air. J Power Sources. 2015;297:504–10.
6. Alberola-Borràs J-A, et al. Relative impacts of methylammonium lead triiodide perovskite solar cells based on life cycle assessment. Sol Energy Mater Sol Cells. 2018;179:169–77.
7. Celik I, et al. Life cycle assessment (LCA) of perovskite PV cells projected from lab to fab. Sol Energy Mater Sol Cells. 2016. https://doi.org/10.1016/j.solmat.2016.04.037.
8. Heo Y-J, et al. Printing-friendly sequential deposition via intra-additive approach for roll-to-roll process of perovskite solar cells. Nano Energy. 2017;41:443–51.
9. Chao L, et al. One-step inkjet printed perovskite in air for efficient light harvesting. Sol RRL. 2018;2:1700217.
10. Yen-Sook J, et al. Progress in scalable coating and roll-to-roll compatible printing processes of perovskite solar cells toward realization of commercialization. Adv Opt Mater. 2018. https://doi.org/10.1002/adom.201701182.
11. Green MA, et al. Solar cell efficiency tables (Version 55). Prog Photovolt Res Appl. 2020;28:3–15.
12. Yi C, et al. Entropic stabilization of mixed A-cation ABX3 metal halide perovskites for high performance perovskite solar cells. Energy Environ Sci. 2016;9:656–62.
13. Eperon GE, Beck CE, Snaith HJ. Cation exchange for thin film lead iodide perovskite interconversion. Mater Horizons. 2015. https://doi.org/10.1039/C5MH00170F.
14. Eperon GE, et al. Formamidinium lead trihalide: a broadly tunable perovskite for efficient planar heterojunction solar cells. Energy Environ Sci. 2014;7:982.
15. Saliba M, et al. Cesium-containing triple cation perovskite solar cells: improved stability, reproducibility and high efficiency. Energy Environ Sci. 2016;9:1989.
16. Tong G, et al. Mixed cation perovskite solar cells by stack-sequence chemical vapor deposition with self-passivation and gradient absorption layer. Nano Energy. 2018;48:536–42.
17. Zhao Y, et al. In situ cesium modification at interface enhances the stability of perovskite solar cells. ACS Appl Mater Interfaces. 2018;10:33205–13.
18. Niemann RG, et al. Cs+ incorporation into CH3NH3PbI3 perovskite: substitution limit and stability enhancement. J Mater Chem A. 2016;4:17819–27.
19. Pering SR, et al. Azetidinium lead iodide for perovskite solar cells. J Mater Chem A. 2017;5:20658–65.
20. Vega E, Mollar M, Marí B. Effect of guanidinium on the optical properties and structure of the methylammonium lead halide perovskite. J Alloys Compd. 2018;739:1059–64.
21. De Marco N, et al. Guanidinium: a route to enhanced carrier lifetime and open-circuit voltage in hybrid perovskite solar cells. Nano Lett. 2016. https://doi.org/10.1021/acs.nanolett.5b04060.
22. Akbulatov AF, et al. Hydrazinium-loaded perovskite solar cells with the enhanced performance and stability. J Mater Chem A. 2016;4:18378–82.
23. Saliba M, et al. Incorporation of rubidium cations into perovskite solar cells improves photovoltaic performance incorporation of rubidium cations into perovskite solar cells improves photovoltaic performance. Science. 2016;354:206–9.
24. Wang L, et al. Potassium-induced phase stability enables stable and efficient wide-bandgap perovskite solar cells. Sol RRL. 2020;4:2000098.
25. Ferdani DW, et al. Partial cation substitution reduces iodide ion transport in lead iodide perovskite solar cells. Energy Environ Sci. 2019;12:2264–72.
26. Ghosh D, Walsh Atkins P, Islam MS, Walker AB, Eames C. Good vibrations: locking of octahedral tilting in mixed-cation iodide perovskites for solar cells. ACS Energy Lett. 2017;2:2424–9.
27. Yi C, et al. Entropic stabilization of mixed A-cation ABX3 metal halide perovskites for high performance perovskite solar cells. Energy Environ Sci. 2015. https://doi.org/10.1039/C5EE03255E.
28. Noh JH, Im SH, Heo JH, Mandal TN, Seok S. Il. Chemical management for colorful, efficient, and stable inorganic-organic hybrid nanostructured solar cells. Nano Lett. 2013;13:1764–9.

29. Davies ML, et al. Compositions, colours and efficiencies of organic–inorganic lead iodide/bromide perovskites for solar cells. Mater Res Innov. 2014;18:482–5.
30. Espinosa N, Serrano-Luján L, Urbina A, Krebs FC. Solution and vapour deposited lead perovskite solar cells: ecotoxicity from a life cycle assessment perspective. Sol Energy Mater Sol Cells. 2015;137:303–10.
31. Babayigit A, et al. Assessing the toxicity of Pb- and Sn-based perovskite solar cells in model organism danio rerio. Sci Rep. 2016;6:18721.
32. Zhai Y, Wang Z, Wang G, Peijnenburg WJGM, Vijver MG. The fate and toxicity of Pb-based perovskite nanoparticles on soil bacterial community: impacts of pH, humic acid, and divalent cations. Chemosphere. 2020;249:126564.
33. Hutter EM, Sangster R, Testerink C, Ehrler B, Gommers CMM. Metal halide perovskite toxicity effects on *Arabidopsis* thaliana plants are caused by iodide ions. iScience. 2022;25:103583.
34. Il Kwak J, Kim L, An Y-J. Sublethal toxicity of PbI2 in perovskite solar cells to fish embryos (Danio rerio and Oryzias latipes): deformity and growth inhibition. Sci Total Environ. 2021;771:145388.
35. Abdelmageed G, et al. Effect of temperature on light induced degradation in methylammonium lead iodide perovskite thin films and solar cells. Sol Energy Mater Sol Cells. 2018;174:566–71.
36. Zhang Y, et al. Intrinsic instability of the hybrid halide perovskite semiconductor CH3NH3PbI3. Chinese Phys Lett. 2018;35:036104.
37. Song Z, et al. Perovskite solar cell stability in humid air: partially reversible phase transitions in the PbI2-CH3NH3I-H2O system. Adv Energy Mater. 2016;6:1600846.
38. Aristidou N, et al. The role of oxygen in the degradation of methylammonium lead trihalide perovskite photoactive layers. Angew Chemie Int Ed. 2015;54:8208–12.
39. Bryant D, et al. Light and oxygen induced degradation limits the operational stability of methylammonium lead triiodide perovskite solar cells. Energy Environ Sci. 2016;9:1655–60.
40. Ponti C, et al. Environmental lead exposure from halide perovskites in solar cells. Trends Ecol Evol. 2022;37:281–3.
41. Saliba M, et al. Cesium-containing triple cation perovskite solar cells: improved stability, reproducibility and high efficiency. Energy Environ Sci. 2016;9:1989–97.
42. Goldschmidt VM. Die gesetze der krystallochemie. Naturwissenschaften. 1926;14:477–85.
43. Kieslich G, Sun S, Cheetham T. Solid-state principles applied to organic-inorganic perovskites: new tricks for an old dog. Chem Sci. 2014;5:4712–5.
44. Travis W, Glover ENK, Bronstein H, Scanlon DO, Palgrave R. On the application of the tolerance factor to inorganic and hybrid halide perovskites: a revised system. Chem Sci. 2016;7:4548–56.
45. Sun Q, Yin W-J. Thermodynamic stability trend of cubic perovskites. J Am Chem Soc. 2017;139:14905–8.
46. Dang Y, et al. Bulk crystal growth of hybrid perovskite material CH3NH3PbI3. CrystEngComm. 2015;17:665–70.
47. Weller MT, Weber OJ, Frost JM, Walsh A. The cubic perovskite structure of black formamidinium lead iodide, α-[HC(NH2)2]PbI3, at 298 K. J Phys Chem Lett. 2015;6:3209–12.
48. Weber OJ, Charles B, Weller MT. Phase behaviour and composition in the formamidinium-methylammonium hybrid lead iodide perovskite solid solution. J Mater Chem A. 2016;4:15375–82.
49. Eames C, et al. Ionic transport in hybrid lead iodide perovskite solar cells. Nat Commun. 2015;6:7497.
50. Weller MT, Weber OJ, Henry PF, Di Pumpo AM, Hansen TC. Complete structure and cation orientation in the perovskite photovoltaic methylammonium lead iodide between 100 and 352 K. Chem Commun. 2015;51:4180–3.
51. Bonadio A, et al. Comparing the cubic and tetragonal phases of MAPbI3 at room temperature. Inorg Chem. 2023;62:7533–44.
52. Quarti C, et al. Structural and optical properties of methylammonium lead iodide across the tetragonal to cubic phase transition: implications for perovskite solar cells. Energy Environ Sci. 2016;9:155–63.
53. Shockley W, Queisser HJ. Detailed balance limit of efficiency of p-n junction solar cells. J Appl Phys. 1961;32:510–9.
54. Brivio F, et al. Lattice dynamics and vibrational spectra of the orthorhombic, tetragonal, and cubic phases of methylammonium lead iodide. Phys Rev B. 2015;92:144308.
55. Onoda-Yamamuro N, Matsuo T, Suga H. Calorimetric and IR spectroscopic studies of phase transitions in methylammonium trihalogenoplumbates (II)†. J Phys Chem Solids. 1990;51:1383–95.
56. Leguy AMA, et al. The dynamics of methylammonium ions in hybrid organic–inorganic perovskite solar cells. Nat Commun. 2015;6:7124.
57. Mosconi E, Amat A, Nazeeruddin MK, Grätzel M, De Angelis F. First-principles modeling of mixed halide organometal perovskites for photovoltaic applications. J Phys Chem C. 2013;117:13902–13.
58. Wang D, Wright M, Elumalai NK, Uddin A. Stability of perovskite solar cells. Sol Energy Mater Sol Cells. 2016;147:255–75.
59. Stoumpos CC, et al. Ruddlesden-popper hybrid lead iodide perovskite 2D homologous semiconductors. Chem Mater. 2016;28:2852–67.
60. Smith IC, Hoke ET, Solis-Ibarra D, McGehee MD, Karunadasa HI. A layered hybrid perovskite solar-cell absorber with enhanced moisture stability. Angew Chemie Int Ed. 2014;53:11232–5.
61. Im J-H, et al. Nanowire perovskite solar cell. Nano Lett. 2015;15:2120–6.
62. Mohammed OF. Outstanding challenges of zero-dimensional perovskite materials. J Phys Chem Lett. 2019;10:5886–8.
63. Grancini G, et al. One-year stable perovskite solar cells by 2D/3D interface engineering. Nat Commun. 2017;8:15684.
64. Azadmanjiri J, Wang J, Berndt CC, Yu A. 2D layered organic-inorganic heterostructures for clean energy applications. J Mater Chem A. 2018. https://doi.org/10.1039/C8TA00132D.
65. Mei A, et al. A hole-conductor–free, fully printable mesoscopic perovskite solar cell with high stability. Sci. 2014;345:295–8.
66. Liu Z, Sun B, Shi T, Tang Z, Liao G. Enhanced photovoltaic performance and stability of carbon counter electrode based perovskite solar cells encapsulated by PDMS. J Mater Chem A. 2016;4:10700–9.
67. Liao G, et al. 15% efficient carbon based planar-heterojunction perovskite solar cells using TiO2/SnO2 bilayer as electron transport layer. J Mater Chem A. 2018. https://doi.org/10.1039/C8TA00526E.
68. Liu S, et al. 17% efficient printable mesoscopic PIN metal oxide framework perovskite solar cells using cesium-containing triple cation perovskite. J Mater Chem A. 2017;5:22952–8.
69. Li X, et al. On-device lead sequestration for perovskite solar cells. Nature. 2020;578:555–8.

70. Horváth E, et al. Fighting health hazards in lead halide perovskite optoelectronic devices with transparent phosphate salts. ACS Appl Mater Interfaces. 2021;13:33995–4002.
71. Mendez LRD, Breen BN, Cahen D. Lead sequestration from halide perovskite solar cells with a low-cost thiol-containing encapsulant. ACS Appl Mater Interfaces. 2022;14:29766–72.
72. Chen S, et al. Preventing lead leakage with built-in resin layers for sustainable perovskite solar cells. Nat Sustain. 2021;4:636–43.
73. Schmidt F, Ledermann L, Schäffer A, Snaith HJ, Lenz M. Rapid sequestration of perovskite solar cell-derived lead in soil. J Hazard Mater. 2022;436:128995.
74. Abundance of elements in the earth's crust and in the sea. In: *CRC Handbook of Chemistry and Physics, 97th edition* 14–17 (2016).
75. Shannon RD. Revised effective ionic radii and systematic studies of interatomic distances in halides and chalcogenides. Acta Crystallogr Sect A. 1976;32:751–67.
76. Kieslich G, Sun S, Cheetham AK. An extended tolerance factor approach for organic–inorganic perovskites. Chem Sci. 2015;6:3430–3.
77. Li J, et al. Biological impact of lead from halide perovskites reveals the risk of introducing a safe threshold. Nat Commun. 2020;11:310.
78. Chiara R, Morana M, Malavasi L. Germanium-based halide perovskites: materials, properties, and applications. ChemPlusChem. 2021;86:879–88.
79. Mitzi DB. Solution-processed inorganic semiconductors. J Mater Chem. 2004;14:2355–65.
80. Mitzi DB, Feild CA, Schlesinger Z, Laibowitz RB. Transport, optical, and magnetic properties of the conducting halide perovskite CH3NH3SnI3. J Solid State Chem. 1995;114:159–63.
81. Mitzi DB, Wang S, Feild CA, Chess CA, Guloy AM. Conducting layered organic-inorganic halides containing <110>-oriented perovskite sheets. Science. 1995;267:1473–6.
82. Chen Z, Wang JJ, Ren Y, Yu C, Shum K. Schottky solar cells based on CsSnI3 thin-films. Appl Phys Lett. 2012;101:93901.
83. Scaife DE, Weller PF, Fisher WG. Crystal preparation and properties of cesium tin(II) trihalides. J Solid State Chem. 1974;9:308–14.
84. Leijtens T, et al. Stability of metal halide perovskite solar cells. Adv Energy Mater. 2015;5:1500963.
85. Sabba D, et al. Impact of anionic Br– substitution on open circuit voltage in lead free perovskite (CsSnI3-xBrx) solar cells. J Phys Chem C. 2015;119:1763–7.
86. Noel NK, et al. Lead-free organic–inorganic tin halide perovskites for photovoltaic applications. Energy Environ Sci. 2014;7:3061–8.
87. Stoumpos CC, Malliakas CD, Kanatzidis MG. Semiconducting tin and lead iodide perovskites with organic cations: phase transitions, high mobilities, and near-infrared photoluminescent properties. Inorg Chem. 2013;52:9019–38.
88. Dimesso L, Fasel C, Lakus-Wollny K, Mayer T, Jaegermann W. Thermal stability of lead-free CH3NH3SnxI3 systems ($0.9 \le x \le 1.1$) for photovoltaics. Mater Sci Semicond Process. 2017;68:152–8.
89. Takahashi Y, et al. Charge-transport in tin-iodide perovskite CH3NH3SnI3: origin of high conductivity. Dalt Trans. 2011;40:5563–8.
90. Chung I, et al. CsSnI3: semiconductor or metal? high electrical conductivity and strong near-infrared photoluminescence from a single material. high hole mobility and phase-transitions. J Am Chem Soc. 2012;134:8579–87.
91. Kubicki DJ, et al. Local structure and dynamics in methylammonium, formamidinium, and cesium tin(II) mixed-halide perovskites from 119Sn solid-state NMR. J Am Chem Soc. 2020;142:7813–26.
92. Weber D. CH3NH3SnBrxI3-x (x = 0–3), ein Sn(II)-system mit kubischer Perowskitstruktur/CH3NH3SnBrxI3-x(x = 0–3), a Sn(II)-system with cubic perovskite structure. Zeitschrift für Naturforsch B. 1978;33:862–5.
93. Koh TM, et al. Formamidinium tin-based perovskite with low Eg for photovoltaic applications. J Mater Chem A. 2015;3:14996–5000.
94. Takahashi Y, Hasegawa H, Takahashi Y, Inabe T. Hall mobility in tin iodide perovskite CH3NH3SnI3: evidence for a doped semiconductor. J Solid State Chem. 2013;205:39–43.
95. Xi J, et al. Multichannel interdiffusion driven FASnI3 film formation using aqueous hybrid salt/polymer solutions toward flexible lead-free perovskite solar cells. Adv Mater. 2017;29:1606964.
96. Ma C, et al. 2D/3D perovskite hybrids as moisture-tolerant and efficient light absorbers for solar cells. Nanoscale. 2016. https://doi.org/10.1039/C6NR04741F.
97. Chunqing M, Dong S, Tsz-Wai N, Ming-Fai L, Chun-Sing L. 2D perovskites with short interlayer distance for high-performance solar cell application. Adv Mater. 2018. https://doi.org/10.1002/adma.201800710.
98. Ran C, et al. Bilateral interface engineering toward efficient 2D–3D bulk heterojunction tin halide lead-free perovskite solar cells. ACS Energy Lett. 2018;3:713–21.
99. Ran C, et al. Conjugated organic cations enable efficient self-healing FASnI3 solar cells. Joule. 2019;3:3072–87.
100. Mitzi DB. Synthesis, crystal structure, and optical and thermal properties of (C4H9NH3)2MI4 (M = Ge, Sn, Pb). Chem Mater. 1996;8:791–800.
101. Takahashi Y, et al. Tunable charge transport in soluble organic-inorganic hybrid semiconductors. Chem Mater. 2007;19:6312–6.
102. Sanchez-Diaz J, et al. Tin perovskite solar cells with >1,300 h of operational stability in N2 through a synergistic chemical engineering approach. Joule. 2022;6:861–83.
103. Krishnamoorthy T, et al. Lead-free germanium iodide perovskite materials for photovoltaic applications. J Mater Chem A. 2015;3:23829–32.
104. Stoumpos CC, et al. Hybrid germanium iodide perovskite semiconductors: active lone pairs, structural distortions, direct and indirect energy gaps, and strong nonlinear optical properties. J Am Chem Soc. 2015;137:6804–19.
105. Thiele G, Rotter HW, Schmidt KD. Kristallstrukturen und phasentransformationen von caesiumtrihalogenogermanaten(II) CsGeX3 (X = Cl, Br, I). Zeitschrift für Anorg und Allg Chemie. 1987;545:148–56.
106. Thiele G, Rotter HW, Schmidt KD. Die kristallstrukturen und phasentransformationen des tetramorphen RbGeI3. Zeitschrift für Anorg und Allg Chemie. 1989;571:60–8.
107. Onoda-Yamamuro N, Yamamuro O, Matsuo T, Suga H. p-T phase relations of CH3NH3PbX3 (X = Cl, Br, I) crystals. J Phys Chem Solids. 1992;53:277–81.
108. Maughan AE, Ganose AM, Scanlon DO, Neilson JR. Perspectives and design principles of vacancy-ordered double perovskite halide semiconductors. Chem Mater. 2019;31:1184–95.
109. Qiu X, et al. From unstable CsSnI3 to air-stable Cs2SnI6: a lead-free perovskite solar cell light absorber with bandgap of 1.48eV and high absorption coefficient. Sol Energy Mater Sol Cells. 2017;159:227–34.

110. Fedorovskiy AE, Drigo NA, Nazeeruddin MK. The role of goldschmidt's tolerance factor in the formation of A2BX6 double halide perovskites and its optimal range. Small Methods. 2020;4:1900426.
111 Tudela D, et al. Mössbauer spectra of tin(IV) iodide complexes. J Chem Soc Dalt Trans. 1999. https://doi.org/10.1039/A905917B.
112. Kaltzoglou A, et al. Optical-vibrational properties of the Cs2SnX6 (X = Cl, Br, I) defect perovskites and hole-transport efficiency in dye-sensitized solar cells. J Phys Chem C. 2016;120:11777–85.
113. Yuan G, et al. Compressibility of Cs2SnBr 6 by X-ray diffraction and raman spectroscopy. Solid State Commun. 2018;275:68–72.
114. Funabiki F, Toda Y, Hosono H. Optical and electrical properties of perovskite variant (CH3NH3)2SnI6. J Phys Chem C. 2018;122:10749–54.
115. Maughan AE, Ganose AM, Almaker MA, Scanlon DO, Neilson JR. Tolerance factor and cooperative tilting effects in vacancy-ordered double perovskite halides. Chem Mater. 2018;30:3909–19.
116. Umedov ST, Khadka DB, Yanagida M, Grigorieva A, Shirai Y. A-site tailoring in the vacancy-ordered double perovskite semiconductor Cs2SnI6 for photovoltaic application. Sol Energy Mater Sol Cells. 2021;230:111180.
117. Al-Muhimeed TI, et al. New lead-free double perovskites X2GeI6 (X = K, Rb, Cs) for solar cells, and renewable energy as an alternate of hybrid perovskites. Int J Energy Res. 2021. https://doi.org/10.1002/er.7022.
118. Saparov B, et al. Thin-film deposition and characterization of a Sn-deficient perovskite derivative Cs2SnI6. Chem Mater. 2016;28:2315–22.
119. Lee B, Krenselewski A, Baik SIL, Seidman DN, Chang RPH. Solution processing of air-stable molecular semiconducting iodosalts, Cs2SnI6–xBrx, for potential solar cell applications. Sustain Energy Fuels. 2017;1:710–24.
120. Lee B, et al. Air-stable molecular semiconducting iodosalts for solar cell applications: Cs2SnI6 as a hole conductor. J Am Chem Soc. 2014;136:15379–85.
121. Chetyrkina MR, et al. Lead, tin, bismuth or organics: assessment of potential environmental and human health hazards originating from mature perovskite PV technology. Sol Energy Mater Sol Cells. 2023;252:112177.
122. Ahmad K, Kumar P, Kim H, Mobin SM. Optoelectronic and photovoltaic properties of (NH4)3Bi2I9: a perovskite-like energy material for Pb-free perovskite solar cells. ChemNanoMat. 2022;8:e202200061.
123. Eckhardt K, et al. Crystallographic insights into (CH3NH3)3(Bi2I9): a new lead-free hybrid organic–inorganic material as a potential absorber for photovoltaics. Chem Commun. 2016;52:3058–60.
124. Lindqvist O. The crystal structure of cesium bismuth iodide, Cs3Bi2I9. Acta Chem Scaninavica. 1968;22:2943–52.
125. Lehner AJ, et al. Crystal and electronic structures of complex bismuth iodides A3Bi2I9 (A = K, Rb, Cs) related to perovskite: aiding the rational design of photovoltaics. Chem Mater. 2015;27:7137–48.
126. The phases of Cs3Bi2I9 between RT and 190 K. Zeitschrift für Krist. - Cryst. Mater. **214**, 279–283 (1999).
127. Sun S, et al. Synthesis, crystal structure, and properties of a perovskite-related bismuth phase, (NH4)3Bi2I9. APL Mater. 2016;4:31101.
128. Sidey VI, Voroshilov YV, Kun SV, Peresh EY. Crystal growth and X-ray structure determination of Rb3Bi2I9. J Alloys Compd. 2000;296:53–8.
129. Hoye RLZ, et al. Methylammonium bismuth iodide as a lead-free, stable hybrid organic-inorganic solar absorber. Chem - A Eur J. 2016;22:2605–10.
130. Park BW, et al. Bismuth based hybrid perovskites A3Bi2I9 (A: methylammonium or cesium) for solar cell application. Adv Mater. 2015;27:6806–13.
131. Waykar R, et al. Environmentally stable lead-free cesium bismuth iodide (Cs3Bi2I9) perovskite: synthesis to solar cell application. J Phys Chem Solids. 2020;146:109608.
132. Lyu M, et al. Organic–inorganic bismuth (III)-based material: a lead-free, air-stable and solution-processable light-absorber beyond organolead perovskites. Nano Res. 2016;9:692–702.
133. Hebig J-C, Kühn I, Flohre J, Kirchartz T. Optoelectronic properties of (CH3NH3)3Sb2I9 thin films for photovoltaic applications. ACS Energy Lett. 2016;1:309–14.
134. Zuo C, Ding L. Lead-free perovskite materials (NH4)3Sb2IxBr 9–x. Angew Chemie Int Ed. 2017;56:6528–32.
135. Harikesh PC, et al. Rb as an alternative cation for templating inorganic lead-free perovskites for solution processed photovoltaics. Chem Mater. 2016;28:7496–504.
136. Sundar S, Chakravarty J. Antimony toxicity. Int J Environ Res Public Health. 2010;7:4267–77.
137. Cooper RG, Harrison AP. The exposure to and health effects of antimony. Indian J Occup Environ Med. 2009;13:3–10.
138. Volonakis G, et al. Lead-free halide double perovskites via heterovalent substitution of noble metals. J Phys Chem Lett. 2016;7:1254–9.
139. Lee DE, Kim SY, Jang HW. Lead-free all-inorganic halide perovskite quantum dots: review and outlook. J Korean Ceram Soc. 2020. https://doi.org/10.1007/s43207-020-00058-5.
140. Slavney AH, Hu T, Lindenberg AM, Karunadasa HI. A bismuth-halide double perovskite with long carrier recombination lifetime for photovoltaic applications. J Am Chem Soc. 2016;138:2138–41.
141. Ghosh B, et al. Superior performance of silver bismuth iodide photovoltaics fabricated via dynamic hot-casting method under ambient conditions. Adv Energy Mater. 2018;8:1802051.
142. Kim Y, et al. Pure cubic-phase hybrid iodobismuthates AgBi2I7 for thin-film photovoltaics. Angew Chemie Int Ed. 2016;55:9586–90.
143. Jain SM, Edvinsson T, Durrant JR. Green fabrication of stable lead-free bismuth based perovskite solar cells using a non-toxic solvent. Commun Chem. 2019;2:91.
144. Ming S, et al. Eco-friendly and stable silver bismuth disulphide quantum dot solar cells via methyl acetate purification and modified ligand exchange. J Clean Prod. 2020;246:118966.
145. Ahmad R, et al. Colloidal lead-free Cs2AgBiBr 6 double perovskite nanocrystals: Synthesis, uniform thin-film fabrication, and application in solution-processed solar cells. Nano Res. 2020. https://doi.org/10.1007/s12274-020-3161-6.
146. Zhang Y, et al. Lead-free double perovskite Cs2AgIn0.9Bi0.1Cl6 quantum dots for white light-emitting diodes. Adv Sci. 2022;9:2102895.
147. Pelle F, Jacquier B, Denis JP, Blanzat B. Optical properties of Cs2NaBiCl6. J Lumin. 1978;17:61–72.
148. Keshavarz M, et al. Tuning the structural and optoelectronic properties of Cs2AgBiBr 6 double-perovskite single crystals through alkali-metal substitution. Adv Mater. 2020. https://doi.org/10.1002/adma.202001878.
149. Lei H, Hardy D, Gao F. Lead-free double perovskite Cs2AgBiBr 6: fundamentals, applications, and perspectives. Adv Funct Mater. 2021. https://doi.org/10.1002/adfm.202105898.
150. Weihua N, et al. Magnetizing lead-free halide double perovskites. Sci Adv. 2022;6:5381.

151. Greul E, Petrus ML, Binek A, Docampo P, Bein T. Highly stable, phase pure Cs2AgBiBr 6 double perovskite thin films for optoelectronic applications. J Mater Chem A. 2017;5:19972–81.
152. Pan W, et al. Cs2AgBiBr 6 single-crystal X-ray detectors with a low detection limit. Nat Photonics. 2017;11:726–32.
153. Yang J, Zhang P, Wei S-H. Band structure engineering of Cs2AgBiBr 6 perovskite through order-disordered transition: a first-principle study. J Phys Chem Lett. 2018;9:31–5.
154. Meneghini C, et al. Nature of ``Disorder'' in the ordered double perovskite ${\mathrm{Sr}}_{2}{\mathrm{FeMoO}}_{6}$. Phys Rev Lett. 2009;103:46403.
155. Schade L, et al. Structural and optical properties of Cs2AgBiBr 6 double perovskite. ACS Energy Lett. 2019;4:299–305.
156. Wei F, et al. The synthesis, structure and electronic properties of a lead-free hybrid inorganic–organic double perovskite (MA) 2KBiCl6 (MA = methylammonium). Mater Horizons. 2016;3:328–32.
157. Shi W, Cai T, Wang Z, Chen O. The effects of monovalent metal cations on the crystal and electronic structures of Cs2MBiCl6 (M = Ag, Cu, Na, K, Rb, and Cs) perovskites. J Chem Phys. 2020;153:141101.
158. Feng H-J, Deng W, Yang K, Huang J, Zeng XC. Double perovskite Cs2BBiX6 (B = Ag, Cu; X = Br, Cl)/TiO2 heterojunction: an efficient Pb-free perovskite interface for charge extraction. J Phys Chem C. 2017;121:4471–80.
159. Volonakis G, et al. Cs2InAgCl6: a new lead-free halide double perovskite with direct band gap. J Phys Chem Lett. 2017;8:772–8.
160. Saeed Y, et al. Cs2NaGaBr 6: a new lead-free and direct band gap halide double perovskite. RSC Adv. 2020;10:17444–51.
161. Yang B, et al. Heteroepitaxial passivation of Cs2AgBiBr 6 wafers with suppressed ionic migration for X-ray imaging. Nat Commun. 2019;10:1989.
162. Jacobs R, Luo G, Morgan D. Materials discovery of stable and nontoxic halide perovskite materials for high-efficiency solar cells. Adv Funct Mater. 2019;29:1804354.
163. Nakajima T, Sawada K. Discovery of Pb-free perovskite solar cells via high-throughput simulation on the K computer. J Phys Chem Lett. 2017;8:4826–31.
164. Filip MR, Giustino F. Computational screening of homovalent lead substitution in organic-inorganic halide perovskites. J Phys Chem C. 2016;120:166–73.
165. Sabzyan H, Ghaderi F. Evaluation of the optical properties of the lead-free mixed-halide iron perovskite CH3NH3FeI2Br for application in solar cells: a computational study. Mater Today Commun. 2021;26:101847.
166. Hakami O. Study of new inorganic double perovskites iodides A2ZrI6 (A = Ga, In, Tl) for solar cells and renewable energy. Int J Energy Res. 2022;46:11326–35.
167. Cucco B, et al. Electronic structure and stability of Cs2TiX6 and Cs2ZrX6 (X = Br, I) vacancy ordered double perovskites. Appl Phys Lett. 2021;119:181903.
168. Pering SR, et al. Investigation of solution-based synthesis of non-toxic perovskite materials using Mg, Ca, Mn, Fe, Cu, and Zn as the B-site cation for photovoltaic applications. J Mater Chem C. 2022;10:14722–8.
169. Wei F, et al. Synthesis, crystal structure, magnetic and electronic properties of the caesium-based transition metal halide Cs3Fe2Br 9. J Mater Chem C. 2018;6:3573–7.
170. Daub M, Ketterer I, Hillebrecht H. Syntheses, crystal structures, and optical properties of the hexagonal perovskites variants ABX3 (B = Ni, A = Gu, FA, MA, X = Cl, Br; B = Mn, A = MA, X = Br). Zeitschrift für Anorg und Allg Chemie. 2018;644:280–7.
171. Sozen Y, Ozen S, Sahin H. Cesium manganese chloride: stable lead-free perovskite from bulk to single layer. J Magn Magn Mater. 2021;531:167845.
172. Chen M, et al. Cesium titanium (IV) bromide thin films based stable lead-free perovskite solar cells. Joule. 2018;2:558–70.
173. Kong D, et al. Solution processed lead-free cesium titanium halide perovskites and their structural, thermal and optical characteristics. J Mater Chem C. 2020;8:1591–7.
174. Ahmad K, Mobin SM. Organic-inorganic copper (II)-based perovskites: a benign approach toward low-toxicity and water-stable light absorbers for photovoltaic applications. Energy Technol. 2020;8:1901185.
175. Li W, Zhu S, Zhao Y, Qiu Y. Structure, electronic and optical properties of Cs2Ti(Br 1-xYx)6 (Y = Cl, I; x = 0, 0.25, 0.5, 0.75, 1) perovskites: the first principles investigations. J Solid State Chem. 2020;284:121213.
176. Li S, et al. Ultrastable lead-free double perovskite warm-white light-emitting devices with a lifetime above 1000 hours. ACS Appl Mater Interfaces. 2020;12:46330–9.
177. Elseman AM, et al. Copper-substituted lead perovskite materials constructed with different halides for working (CH3NH3)2CuX4-based perovskite solar cells from experimental and theoretical view. ACS Appl Mater Interfaces. 2018;10:11699–707.
178. Li X-L, Li Z, Zhang G, Yang G-J. Lead-free perovskite [H3NC6H4NH3] CuBr 4 with both a bandgap of 1.43 eV and excellent stability. J Mater Chem A. 2020;8:5484–8.
179. Kozhina II, Korol'kov DV. X-ray diffraction study of rubidium and cesium bromotitanates. J Struct Chem. 1965;6:84–9.
180. Beegum KAB, Sasi S, Mathew A, Asha AS, Reshmi R. Nano fibers of lead free perovskite cesium titanium bromide ($CsTiBr_3$) thin films by in-house deposition technique. Phys Scr. 2021;96:55707.
181. Maddah HA, Berry V, Behura SK. Cuboctahedral stability in titanium halide perovskites via machine learning. Comput Mater Sci. 2020;173:109415.
182. Chakraborty K, Choudhury MG, Paul S. Study of physical, optical, and electrical properties of cesium titanium (IV)-based single halide perovskite solar cell. IEEE J Photovoltaics. 2021;11:386–90.
183. Aslam S, Farooqi AS, Rahman MYA, Samsuri SAM. Titanium-based vacancy-ordered double halide family in perovskite solar cells. Phys Stat Sol. 2022;219:2100671.
184. Euvrard J, Wang X, Li T, Yan Y, Mitzi DB. Is Cs2TiBr 6 a promising Pb-free perovskite for solar energy applications? J Mater Chem A. 2020;8:4049–54.
185. Mendes JL, et al. Interfacial states, energetics, and atmospheric stability of large-grain antifluorite Cs2TiBr 6. J Phys Chem C. 2020;124:24289–97.
186. Futscher MH, Gangishetty MK, Congreve DN, Ehrler B. Manganese doping stabilizes perovskite light-emitting diodes by reducing ion migration. ACS Appl Electron Mater. 2020;2:1522–8.

187. Liu W, et al. Efficient perovskite solar cells fabricated by manganese cations incorporated in hybrid perovskites. J Mater Chem C. 2019;7:11943–52.
188 Liu M, et al. Manganese doping promotes the synthesis of bismuth-based perovskite nanocrystals while tuning their band structures. Small. 2021. https://doi.org/10.1002/smll.202100101.
189. Kestigian M, Holloway WW Jr. The preparation, single-crystal-growth, and fluorescence studies of divalent manganese chlorides of rubidium and cesium. Phys Stat Sol. 1971;6:K19–22.
190. Depmeier W, Klaska K-H. The structure of manganese methylammonium trichloride dihydrate, a member of the CsMnCl3.2H2O family, at room temperature. Acta Crystallogr Sect B. 1980;36:1065–8.
191. Nie Z, et al. Layered and Pb-Free organic-inorganic perovskite materials for ultraviolet photoresponse: (010)-oriented (CH3NH3)2MnCl4 thin film. ACS Appl Mater Interfaces. 2016;8:28187–93.
192. Visser D, Verschoor GC, IJdo DJW. The structure of KNiCl3 at room temperature. Acta Crystallogr Sect B. 1980;36:28–34.
193. Raw AD, Ibers JA, Poeppelmeier KR. Syntheses and structure of hydrothermally prepared CsNiX3 (X=Cl, Br, I). J Solid State Chem. 2012;192:34–7.
194. Willett RD. Crystal structure of CH3NH3NiCl3. J Chem Phys. 1966;45:3737–40.
195. Ramirez D, Jaramillo F, Pérez-Walton S, Osorio-Guillén JM. New nickel-based hybrid organic/inorganic metal halide for photovoltaic applications. J Chem Phys. 2018;148:244703.
196. Daub M, Stroh R, Hillebrecht H. Synthesis, crystal structure, and optical properties of (CH3NH3)2CoX4 (X = Cl, Br, I, Cl0.5Br 0.5, Cl0.5I0.5, Br.05I0.5). Zeitschrift für Anorg und Allg Chemie. 2016;642:268–74.
197. Salah A. Ben, Bats JW, Kalus R, Fuess H, Daoud A. Crystal structure determination of complexes of monomethylammonium chloride and mercury(II) chloride: CH3NH3HgCl3, (CH3NH3)2HgCl4, and CH3NH3Hg2Cl5. ZAAC J Inorg Gen Chem. 1982;493:178–86.
198. Morosin B, Emerson K. Monomethylammonium tetrachlorozincate (II). Acta Crystallogr Sect B. 1976;32:294–5.
199. Elattar A, et al. Single crystals of mixed-cation copper-based perovskite with trimodal bandgap behavior. Chem - A Eur J. 2022;28:e202104316.
200. Krüger N, et al. Stable phases of the Cs2CuCl4–xBrx mixed systems. Cryst Growth Des. 2010;10:4456–62.
201. Cortecchia D, et al. Lead-free MA2CuClxBr 4–x hybrid perovskites. Inorg Chem. 2016;55:1044–52.
202. Pabst I, Fuess H, Bats JW. Structure of monomethylammonium tetrachlorocuprate at 297 and 100 K. Acta Crystallogr. 1987;43:413–6.
203. Abfalterer A, et al. Colloidal Synthesis and Optical Properties of Perovskite-Inspired Cesium Zirconium Halide Nanocrystals. ACS Mater Lett. 2020;2:1644–52.
204. Engel G. Die kristallstrukturen einiger hexachlorokomplexsalze. Zeitschrift für Krist Cryst Mater. 1935;90:341–73.
205. Ning, W. *et al.* Magnetizing lead-free halide double perovskites. *Sci. Adv.* **6**, eabb5381 (2023).
206. Hoye RLZ, et al. Fundamental carrier lifetime exceeding 1 µs in Cs2AgBiBr 6 double perovskite. Adv Mater Interfaces. 2018;5:1800464.
207. Wang B, et al. Chlorophyll derivative-sensitized TiO2 electron transport layer for record efficiency of Cs2AgBiBr 6 double perovskite solar cells. J Am Chem Soc. 2021;143:2207–11.
208. Kopacic I, et al. Enhanced performance of germanium halide perovskite solar cells through compositional engineering. ACS Appl Energy Mater. 2018;1:343–7.